BAJOPAS Volume 15 Number 1, June, 2022

http://dx.doi.org/10.4314/bajopas.v15i1.27

Bayero Journal of Pure and Applied Sciences, 15(1): 187 - 194
Received: February, 2022
Accepted: April, 2022
ISSN 2006 – 6996

NUMERICAL INVESTIGATION ON ENERGY CONVERSION EFFICIENCY OF LEAD-BASED PEROVSKITE SOLAR CELLS USING DIFFERENT TRANSPARENT CONDUCTIVE OXIDES

Sani, F.[1] and Musa, A.O.[2]
[1]Department of Physics, Usmanu Danfodiyo University, Sokoto, Nigeria.
[2]Department of Physics, Bayero University Kano, Nigeria.
Correspondence: faruk.sani@udusok.edu.ng, Tel.: +234-803-401-5827

ABSTRACT
Perovskite solar cells have attracted tremendous attention owing to its rapid increase in power conversion efficiency. This work designed and simulated lead-based perovskite solar cells in planar structure; TCO/ TiO_2/ $CH_3NH_3PbI_3$/Spiro-OMeTAD/Au. To study the effect of various transparent conductive oxides (TCOs) on power conversion efficiency of the devices, Solar Capacitance (SCAP) simulating software was used. To achieve an optimum efficiency, the influence of thickness and band-gap energy of the absorber layer were varied and investigated. The optimized power conversion efficiency (PCE) is achieved using MoO_3/TiO_2/$CH_3NH_3PbI_3$/Spiro-OMeTAD/Au architecture with PCE of 22.44 % and V_{oc}, J_{sc}, and FF of 1.0842 V, 25.57 mA/cm^2 and 80.94 % respectively. The numerical simulation shows the potential of substituting the conventional FTO and ITO used in perovskite solar cells with MoO_3 as a promising transparent conductive oxide layer.
Keywords: boron-doped zinc oxide, efficiency, molybdenum oxide, perovskite, solar cells.

INTRODUCTION

Recently, halide perovskite-based solar cells show a great photovoltaic performance owing to their high absorption coefficient and simple method of fabrication (Chen *at al.*, 2015; Green *et al.*, 2014). The power conversion efficiency increases rapidly to the recent value of 25.2 % (nrel, 2021). Doped and un-doped transparent conductive oxide has been utilized as a basic component in the fabrication of perovskite solar cells (PSCs). Transparent conductive oxide with high band-gap transmits 80 % of visible light (Bawaked *et al.*, 2014; Bhachu *et al.*, 2012; Sthasivam *et al.*, 2015). Fluorine-doped tin oxide [FTO] and indium-doped tin oxide (ITO) have been regularly used as transparent conductive oxide (TCO) in perovskite solar cells due to their low resistivity and high transparency (Noel *et al.*, 2014; Hao *et al.*, 2014; Hao *et al.*, 2015; Yokoyama *et al.*, 2016; Fujihara *et al.*, 2017; Yu *et al.*, 2016; Peng *et al.,* 2020). However, it was reported that indium metal is a rare and toxic material (Dianetti *et al.*, 2015; Hagendorfer *et al.*, 2014; Minami, 2005; Sibinski *et al.*, 2012; Sohn and Kim, 2011). Furthermore, fluorine-doped tin oxide has relatively low electrical conductivity and high leakage current (Liu *et al.*, 2010).

To further explore a substitute to the conventional TCOs, this work aimed to design and simulate lead-based perovskite solar cells in planar structure employing different TCOs, Molybdenum trioxide (MoO_3), boron-doped zinc oxide (BZO) and zinc oxide (ZnO) as transparent conductive layer. To achieve an optimum photovoltaic performance, the influence of thickness, defect density and operating temperature of the TCO were investigated. The schematic device architecture is presented in Figure 1.

MATERIALS AND DEVICE MODELING

Materials

Methyl-ammonium lead iodide ($CH_3NH_3PbI_3$) used as light absorbing layer, titanium dioxide (TiO_2) and Spiro-OMeTAD used as Electron Transporting Layer (ETL) and Hole Transporting Layer (HTL) respectively, boron-doped zinc oxide (BZO), Zinc Oxide (ZnO) and Molybdenum trioxide (MoO_3) were employed as front contact and Gold (Au) was selected as back contact as shown in Figure 1.

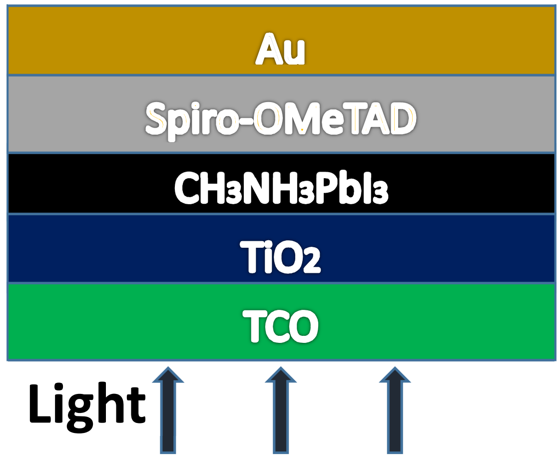

Figure 1. Schematic architecture of the device

The simulation parameters of those layers were obtained from previous literature (Patel, 2012; Baig *et al*., 2018; Azri *et al*., 2019; Minemoto and Murata, 2014; Teimouri and Muhammad, 2018; Slami *et al*., 2020; Bedia *et al*., 2014; Raudik *et al*., 2018; Baba *et al*., 2018; Rahman, 2021; Ouedraogo *et al*., 2013; Zaid *et al*., 2019; Mozafari and Shahhoseini, 2020; Ghazi *et al*., 2021) and were tabulated in Table 1.

Device Modeling

In this study, the device modeling was conducted using SCAPS (SCAPS 3.3.10 version) software. The spectrum used is AM1.5G with an incident power density of 1000 W/cm^2 (1 Sun). Furthermore, the work point bias 0 V, frequency of $1.0\ X\ 10^6\ Hz$ were adopted. SCAPS is 1D solar cell simulation program. It works by solving the Poisson equations and the continuity equations for electrons and holes, and carrier transport (Movla, 2014). The simulation procedure is shown in Figure 2.

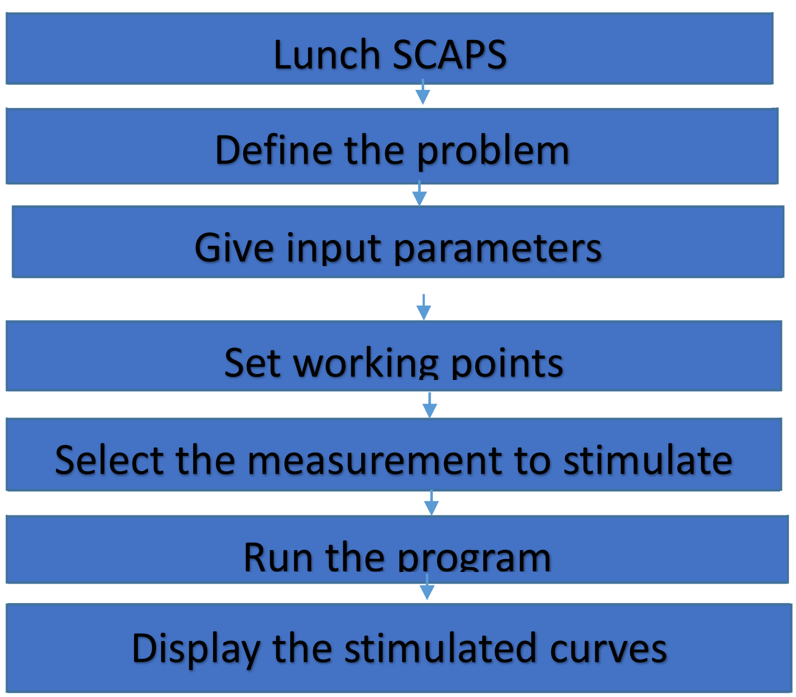

Figure 2. Simulation step-by-step procedure

Table 1. Input parameters for simulation of $CH_3NH_3PbI_3$ performance

Parameters	**BZO**	**ZnO**	**MoO_3**	**TiO_2**	**$CH_3NH_3PbI_3$**	**Spiro-OMeTAD**
Thickness (nm)	200	200	200	100	300 (varied)	200
Band gap, E_g (eV)	3.3	3.3	3.8	3.2	1.55	3.0
Electron affinity, X (eV)	4.55	4.6	4.1	3.9	3.9	2.45
Relative dielectric permittivity, Ɛr	9	9	9	9.0	6.25	3.0
CB effective density of states, N_c (cm^{-3})	3 $x10^{18}$	4 $x10^{18}$	2.2 $x10^{18}$	1 x 10^{21}	2.2 $X10^{19}$	1 x 10^{19}
VB effective density of states, N_v (cm^{-3})	$1.8x10^{19}$	2 $x10^{19}$	1.8 $x10^{19}$	2 x 10^{20}	1.8 X 10^{19}	1 x 10^{19}
Electron mobility, μ_n (cm^2/Vs)	100	100	30	20	2	0.0002
Hole mobility, μ_p (cm^2/Vs)	31	25	6	10	2	0.0002
Donor concentration, N_d (cm^{-3})	10^{20}	$1x10^{17}$	$1x10^{17}$	1 x 10^{19}	10^{16}	0
Acceptor concentration, N_a (cm^{-3})	0	0	0	0	0	1 x 10^{18}
Defect density, N_t (cm^{-3})	$1x10^{14}$	$1x10^{14}$	$1x10^{14}$	1 x 10^{15}	2.5 x 10^{13}	1 x 10^{15}

RESULTS AND DISCUSSION

Influence of TCO on the device performance

The simulated J-V curves and the photovoltaic parameters obtained for the devices by employing the three different TCOs are presented in Figure 3 and Table 2 respectively. From Table 2, it is found that the devices with the MoO_3 and BZO show the highest power conversion efficiencies in contrast to the device with the ZnO which exhibits the lowest power conversion efficiencies. The results show that the undoped ZnO has low optical transmission to be used as TCO. Therefore, the impurity-doped ZnO is more suitable for TCO which is in line with the findings of (Chen *et al.*, 2014). Furthermore, the output results indicate that there is insignificant difference in PCE achieved by MoO_3 and BZO based devices. This signifies that both TCOs (MoO_3 and BZO) have high optical transmission appropriate to be used as front contact for the fabrication of PSCs.

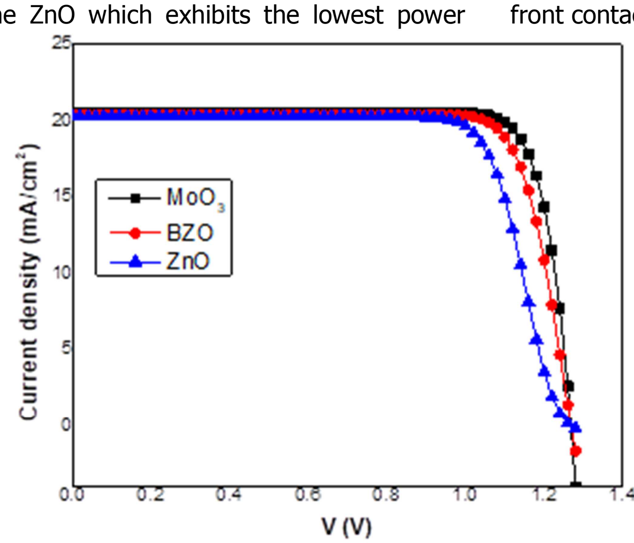

Figure 3. Influence of various TCOs on the J-V characteristics

Table 2. Photovoltaic parameters achieved using various TCOs

TCO	Voc (V)	Jsc (mA/cm^2)	FF (%)	η (%)
MoO_3	1.2685	20.55	80.06	21.91
BZO	1.2689	20.40	81.44	21.08
ZnO	1.2685	20.27	76.37	19.64

Effect of Absorber Thickness on the Performance of the Devices

The thickness of the absorber layer was varied from 400 nm to 1200 nm with the three selected TCOs (MoO_3/BZO/ZnO/TiO_2/$CH_3NH_3PbI_3$/Spiro-OMeTAD/Ag) and the remaining input parameters remain unchanged. The J-V characteristic curves obtained for the three devices are presented in Figure 4 and the photovoltaic performance are elucidated in Tables 3, 4 and 5. From the photovoltaic performances of all the devices, it could be seen clearly that the J_{sc} increases with increasing thickness of the absorber layer from 400 nm to 1200 nm. This is because large amount of photons will be absorbed by the layer. Hence, the excitation of excess charge carrier concentration causes the Jsc and the efficiency to increase as well (Koh *et al.,* 2015). However, it is observed from the results that there is a decrease in Voc as the thickness increased. An increase in the absorber layer thickness results to lager recombination rate due to long diffusion length as reported by (Stanic *et al.*, 2021). The optimal performance was achieved using MoO_3 as TCO with the highest PCE of 26.51 % and V_{oc}, J_{sc}, and FF of 1.2096 V, 25.87 mA/cm^2 and 84.70 % respectively.

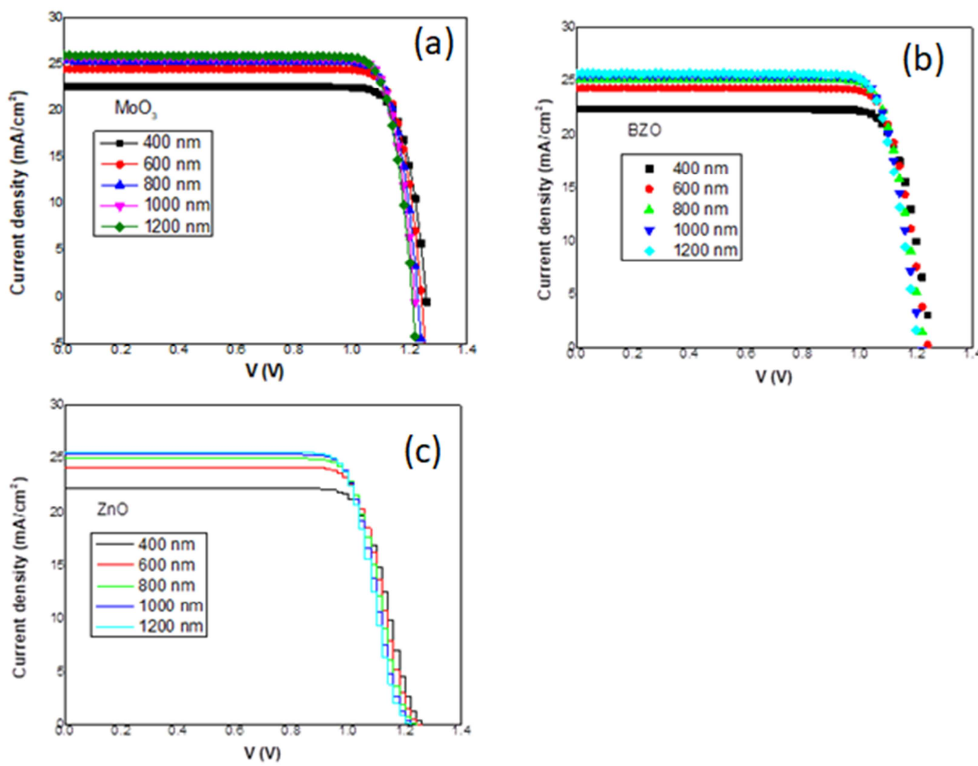

Figure 4. Effect of absorber layer thickness on the J-V characteristics using various TCO: (a) MoO_3, (b) BZO, and (c) ZnO.

Table 3. Electrical outputs obtained at varied absorber layer thickness using MoO_3 as TCO

Thickness (nm)	Voc (V)	Jsc (mA/cm^2)	FF (%)	PCE (%)
400	1.2583	22.50	84.06	23.80
600	1.2418	24.46	84.18	25.57
800	1.2288	25.31	84.32	26.22
1000	1.2184	25.70	84.52	26.46
1200	1.2096	25.87	84.70	26.51

Table 4. Electrical outputs obtained at varied absorber layer thickness using BZO as TCO

Thickness (nm)	Voc (V)	Jsc (mA/cm^2)	FF (%)	PCE (%)
400	1.2586	22.34	81.29	22.86
600	1.2421	24.31	81.23	24.53
800	1.2293	25.15	81.34	25.15
1000	1.2187	25.54	81.44	25.35
1200	1.2100	25.72	81.58	25.39

Table 5. Electrical outputs obtained at varied absorber layer thickness using ZnO as TCO

Thickness (nm)	Voc (V)	Jsc (mA/cm^2)	FF (%)	PCE (%)
400	1.2586	22.21	76.10	21.28
600	1.2421	24.18	75.92	22.80
800	1.2290	25.02	75.94	23.35
1000	1.2188	25.41	76.02	23.54
1200	1.2097	25.58	76.15	23.57

Effect of Absorber Layer Band-Gap on the Performance of the Devices

One of the unique properties of the organic-inorganic halide perovskite is the tunable band gap. Band gap significantly affect the optical absorption of the light absorbing material. It has been reported that the band-gap energy of $CH_3NH_3PbI_3$ ranged between 1.45 eV to 1.7 eV (Lin et al., 2017, Casas *et al*., 2017; Karimi and Ghorashi, 2017). The effect of band-gap on the device performance was numerically investigated by changing the band-gap from 1.4eV to 1.7eV. The J-V characteristic curves and the electrical parameters obtained for the three devices are presented in Figure 5 and Tables 6, 7, and 8. The results show decrease in Jsc as the absorber layer band-gap increased. This might be due to increased series resistance as the band-gap increased resulting to rapid drop in the J_{sc} and efficiency of the devices. The output results also indicates that Voc and FF increase with the increasing the band-gap. This can be explained that after electron-hole is generated by the absorber layer, the electrons and holes are separated by a greater energy barrier apart. Hence this leads V_{oc} to increase as suggested by (Bishnoi and Pandey, 2018). However, the best device performance was realized using MoO_3 at 1.4 eV with the highest efficiency of 22.44 % and V_{oc}, J_{sc}, and FF of 1.0842 V, 25.57 mA/cm^2 and 80.94 % respectively.

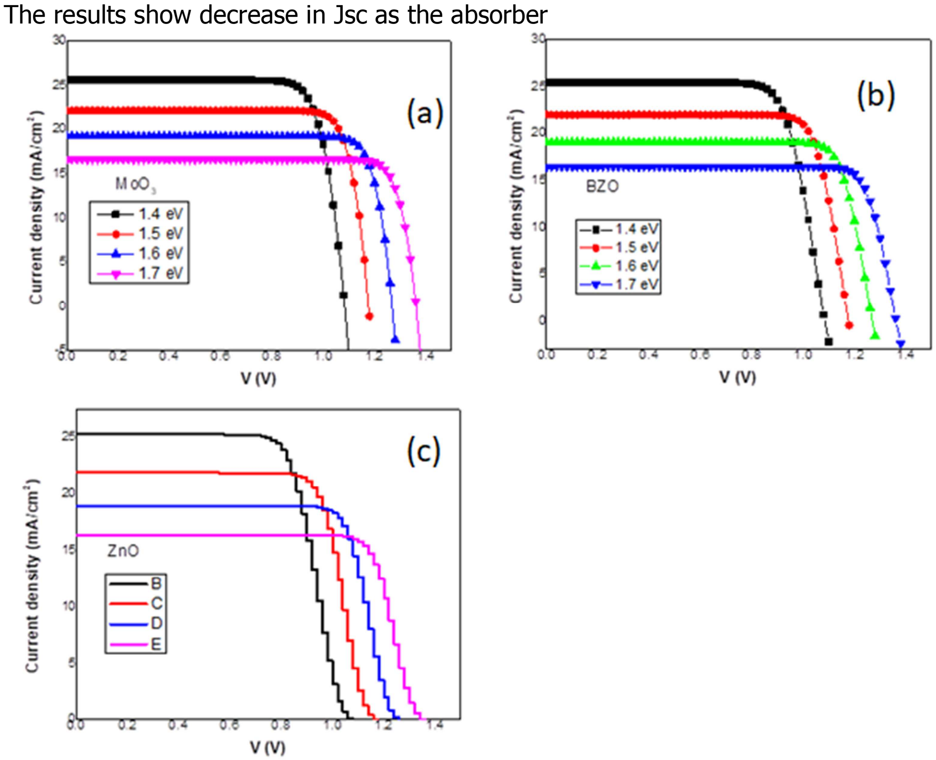

Figure 5. Effect of absorber layer band-gap on the J-V characteristics using various TCO: (a) MoO_3, (b) BZO, and (c) ZnO

Table 6. Electrical outputs obtained at varied absorber layer thickness using MoO_3 as TCO

Band-gap (eV)	Voc (V)	Jsc (mA/cm^2)	FF (%)	PCE (%)
1.4	1.0842	25.57	80.94	22.44
1.5	1.1769	22.17	83.93	21.90
1.6	1.2689	19.22	85.26	19.54
1.7	1.3621	16.63	86.26	19.54

Table 7. Electrical outputs obtained at varied absorber layer thickness using BZO as TCO

Band-gap (eV)	Voc (V)	Jsc (mA/cm^2)	FF (%)	PCE (%)
1.4	1.0846	25.42	77.53	21.38
1.5	1.1772	22.02	80.20	20.20
1.6	1.2693	19.07	82.74	20.03
1.7	1.3623	16.49	84.14	18.90

Table 8. Electrical outputs obtained at varied absorber layer thickness using ZnO as TCO

Band-gap (eV)	Voc (V)	Jsc (mA/cm^2)	FF (%)	PCE (%)
1.4	1.0845	25.30	71.50	19.61
1.5	1.1770	21.89	75.48	19.45
1.6	1.2689	18.94	77.70	18.69
1.7	1.3623	16.36	79.49	17.71

CONCLUSION

In this work, numerical simulation of lead-based perovskite solar cells employing various TCOs such as MoO_3, BZO and ZnO were investigated using SCAPS Simulating software. The device performances were also studied against varied thickness and band-gap energy of the absorber layer. Absorber layer thickness optimization results show that 1200 nm thickness is the optimum thickness value to achieve best photovoltaic performance for the studied perovskite solar cells architectures. Furthermore, the study provides theoretical highlights towards achieving efficient perovskite solar cells by tuning the band-gap energy of the absorber layer. However, the best optimized result is realized using MoO_3 as TCO with efficiency of 22.44 %. It can be concluded that MoO_3 has the ability to substitute conventional FTO and ITO in perovskite solar cells.

Author contributions: F. Sani designed and simulated the perovskite-based solar cells and A.O. Musa revised the findings of the research. All authors contributed to the final version of the manuscript.

Conflicts of Interest: The authors declare no conflict of interest.

REFERENCES

Azri, F., Meftah, A., Sengouga, N. and Meftah, A. (2019). Electron and hole transport layers optimization by numerical simulation of a perovskite solar cell. *Sol. Energy*, 181: 372–378.

Baba, B.J., Mandapu, U. Vedanayakam, V. and Tyagarajan, K. (2018). Optimization of high efficiency tin halide perovskite solar cells using SCAPS-1D. *International journal of simulation and process modelling,* 13(3):221, doi: 10.150/IJSPM.2018.10014179.

Baig, F., Khattak, Y.H., Marí, B., Beg, S., Ahmed, A. and Khan, K. (2018). Efficiency Enhancement of $CH_3NH_3SnI_3$ Solar Cells by Device Modeling. *J. Electron. Mater.*,47: 5275 - 5282.

Bawaked, S.M., Sathasivam, S., Bhachu, D.S., Chadwick, N., Obaid, A.Y., Al-Thabaiti,S., Basahel, S.N., Carmalt, C.J., Parkin, I.P., 2014. Aerosol assisted chemical vapor deposition of conductive and photocatalytically active tantalum doped titanium dioxide films. *J. Mater. Chem. A* 2, 12849. http://dx.doi.org/10.1039/C4TA01618A.

Bedia, F.Z., Bedia, A., Aillerie, M., Maloufi, N., Genty, F. and Benyocef, B. (2014). Influence of Al-doped ZnO transparent contacts deposited by a spray pyrolysis technique on performance of HIT solar cells. *Energy procedia*, (50): 853-861, doi: 10.1016/j.egypro.2014.06.104.

Bhachu, D.S., Sankar, G. and Parkin, I.P. (2012). Aerosol assisted chemical vapor deposition of transparent conductive zinc oxide films. *Chem. Mater*. 24: 4704–4710. http://dx.doi.org/10.1021/cm302913b

Bishnoi, S. and Pandey, S.K. (2018). Device performance analysis for lead-free perovskite solar cell optimization. *IET Optoelectronics*, 12(4): 185 – 190.

Casas, G. A., Cappelletti, M. A., Cédola, A. P., Soucase, B. M. and Blancá, E. P. (2017).

Analysis of the power conversion efficiency of perovskite solar cells with different materials as Hole-Transport Layer by numerical simulations. *Superlattices and Microstructures,* 107: 136-143.

Chen, J., Chen, D., Zhou, Y., Li, W., Yanjie, R. and Hu, L. (2014). Electrochemical deposition of Al-doped ZnO transparent conducting nanowires arrays for thin-film solar cell electrodes. *Mater. Lett.,* 117: 162-164.

Chen. Q., Marco. N.D., Yang. Y., Song. T.B., Chen. C.C., Zhou. H. and Yang. Y. (2015). Under the Spotlight: The Organic-Inorganic Hybrid Halide Perovskite for Optoelectronic Applications. *Nano Today*, 10: 355-396.

Dianetti, M., Di Giacomo, F., Polino, G., Ciceroni, C., Liscio, A., D'Epifanio, A., Licoccia, S., Brown, T.M., Di Carlo, A., Brunetti, F. (2015). TCO-free flexible organo metal trihalide perovskite planar-heterojunction solar cells. Sol. *Energy Mater. Sol. Cells,* 140, 150–157

Fujihara, T., Terakawa, S., Matsushima, T., Qin, C., Yahiro, M. and Adachi, C. (2017). Fabrication of high coverage $MASnI_3$ perovskite films for stable, planar heterojunction solar cells. *J. Mater. Chem. C.,* 5: 1121–1127.

Ghazi, A.N., Khizer, J., Yasir, U., Muhammad, W.S. and Muhammad, K. (2021). Numerical Modeling and Optimization of Perovskite Silicon Tandem Solar Cell Using SCAPS-1D. *Sch. Bull*, 7(7): 171 – 184.

Green. M. A., Ho-Baillie, A. and Snaith. H. J. (2014). The emergence of perovskite solar cells. *Nature Photonics*, *8*(7): 506–514.

Hagendorfer, H., Lienau, K., Nishiwaki, S., Fella, C.M., Kranz, L., Uhl, A.R., Jaeger, D., Luo, L., Gretener, C., Buecheler, S., Romanyuk, Y.E., Tiwari, A.N. (2014). Highly transparent and conductive ZnO: Al thin films from a low temperature aqueous solution approach. *Adv. Mater*. 26: 632–636.

Hao, F., Stoumpos, C.C., Cao, D.H., Chang, R.P. and Kanatzidis, M.G. (2014). Lead-free solid-state organic–inorganic halide perovskite solar cells. *Nat. Photonics* 8, 489.

Hao, F., Stoumpos, C.C., Guo, P., Zhou, N., Marks, T.J., Chang, R.P. and Kanatzidis, M.G. (2015). Solvent-mediated crystallization of $CH_3NH_3SnI_3$ films for heterojunction depleted perovskite solar cells. *J. Am. Chem. Soc*. 137: 11445–11452.

Karimi, E. and Ghorashi, S. M. B. (2017). Investigation of the influence of different hole-transporting materials on the performance of perovskite solar cells. *Optik-International Journal for Light and Electron Optics*, 130: 650-658.

Koh, T. M., Krishnamoorthy, T., Yantara, N., Shi, C., Leong, W.L., Pablo, P.B., Grimsadale, A.C., Mhaisalkar,S.G. and Mathews, N. (2015). Formamidinium tin-based perovskite with low E g for photovoltaic applications. *Journal of Materials Chemistry A* 3: 14996-15000.

Lin, L., Jiang, L., Qiu, Y. and Yu, Y. (2017). Modeling and analysis of HTM-free perovskite solar cells based on ZnO electron transport layer. *Superlattices and Microstructures*, 104: 167-177.

Liu, H., Avrutin, V., Izyumskaya, N., Özgr, Ü., Morkoç, H., (2010). Transparent conducting oxides for electrode applications in light emitting and absorbing devices. *Superlatt. Microstruct*. 48, 458–484.

Minami, T. (2005). Transparent conducting oxide semiconductors for transparent electrodes. *Semicond. Sci. Technol.* 20, S35–S44

Minemoto, T. and Murata, M. (2014). Impact of work function of back contact of perovskite solar cells without hole transport material analyzed by device simulation. *Curr. Appl. Phys.*, 14: 1428–1433.

Movla, H. (2014). Optimization of the CIGS based thin film solar cells: numerical simulation and analysis. *Optik*. 125(1): 67–70.

Mozafari, B. and Shahhoseini (2020). Using Molybdenum trioxide as a TCO layer to improve performance of CdTe/CdS thin film solar cell. *Signal processing and Renewable Energy*, pp 57-65.

Noel, N.K., Stranks, S.D., Abate, A., Wehrenfennig, C., Guarnera, S., Haghighirad, A.-A., Sadhanala, A., Eperon, G.E., Pathak, S.K. and Johnston, M.B. (2014). Lead-free organic–inorganic tin halide perovskites for photovoltaic applications. *Energy Environ. Sci*.7: 3061–3068.

nrel-research-pushes-perovskites-closer-to-market @ www.nrel.gov.https://www.nrel.gov/new s/program/2021/new-perovskite-design-shows-path-to-higher-efficiency.html (Retrieved May 25, 2021).

Ouedraogo, S., Zougmore, F. and Ndjaka. J.M. (2013). Numerical analysis of copper-indium-Gallium-Diselinide-based solar cells by SCAPS-1D. *International journal of photoenergy*, vol., 421076, doi: 10.1155/2013/421076.

Patel. P.K. (2012). Device simulation of highly efficient eco-friendly $CH_3NH_3SnI_3$ perovskite solar cell. *Scientific reports*, 11,3082, doi:10.1038/s41598-021-828-w

Peng, L. and Xie, W. (2020).Theoretical and experimental investigations on the bulk photovoltaic in lead-free perovskites $MASnI_3$ and $FASnI_3$. *RSC Adv.*, 10: 14679–14688

Rahman, M.A. (2021). Design and simulation of a high performance Cd-free Cu_2SnSe_3 solar cells with SnS electron-blocking hole transport later by SCAPS-1D. *SN Applied sciences*, 3253, doi: 10.1007/s42452-021-04267-3.

Raudik, S.A., Mozharov, A.M., Mitin, D.M., Bolshakov, A.D., Rajanna, P.M., Nasibulin, A.G. and Mukhin, I.S. (2018). Numerical simulation of the carbon nanotubes transport layer influence on performance of GaAs solar cells. *IOP conf. series: Journal of physics*, doi: 10.1088/1742-6596/1124/4/041040.

Sathasivam, S., Bhachu, D.S., Lu, Y., Chadwick, N., Althabaiti, S.a., Alyoubi, A.O., Basahel, S.N., Carmalt, C.J., Parkin, I.P., 2015. Tungsten doped TiO2 with enhanced photocatalytic and optoelectrical properties via aerosol assisted chemical vapor deposition. *Sci. Rep.* 5, 10952. http://dx.doi.org/10.1038/srep10952

Sibin´ski, M., Znajdek, K., Walczak, S., Słoma, M., Górski, M., Cenian, A. (2012).Comparison of ZnO:Al, ITO and carbon nanotube transparent conductive layers in flexible solar cells applications. *Mater. Sci. Eng. B Solid-State Mater. Adv.Technol.* 177: 1292–1298.

Slami. A., Bouchaour. M. and Merad. L. (2020). Comparative Study of Modelling of Perovskite Solar Cell with Different HTM Layers. *International Journal of Materials*, vol. 7. DOI:10.46300/91018.2020.7.1

Sohn, S. and Kim, H. (2011). Transparent conductive oxide (TCO) films for organic light emissive devices (OLEDs). Org. Light Emit. Diode – *Mater. Process Dev.*, 233–274

Stanic, D., Kojic, V., Cižmar, T., Juraic, K., Bagladi, L., Mangalam,J., Rath, T. andGajovic, A.(2021). Simulating the Performance of a Formamidinium Based Mixed Cation Lead Halide Perovskite Solar Cell. *Materials*, 14, 6341. https://doi.org/10.3390/ma14216341.

Teimouri, R. and Mohammadpour, R. (2018). Potential application of $CuSbS_2$ as the hole transport material in perovskite solar cell: A simulation study. *Superlattices Microstructure*, 118: 116–122.

Yokoyama, T., Cao, D.H., Stoumpos, C.C., Song, T.-B., Sato, Y., Aramaki, S. and Kanatzidis, M.G. (2016). Overcoming short-circuit in lead-free $CH_3NH_3SnI_3$ perovskite solar cells via kinetically controlled gas–solid reaction film fabrication process. *J. Phys. Chem. Lett.* 7: 776–782

Yu, Y., Zhao, D., Grice, C.R., Meng, W., Wang, C., Liao, W., Cimaroli, A.J., Zhang, H., Zhu, K. and Yan, Y. (2016). Thermally evaporated methyl-ammonium tin triiodide thin films for lead-free perovskite solar cell fabrication. *RSC Adv.*, 6: 90248–90254.

Zaid, B. Ullah, M.S., Hadjoudja, B. and Gagui, S. (2019). Role of TC films in improving the efficiency of Cds/MoS_2 heterojunction solar cells. *Journal of Nano and Electronic Physics*, 11(2): 02030, doi: 10.21272/jnep.11(2).02030.